Materials Today Bio 31 (2025) 101624

Contents lists available at ScienceDirect

Materials Today Bio

journal homepage: www.journals.elsevier.com/materials-today-bio

Poly(glycerol succinate) hydrogel promotes spinal cord repair by regulating bio-energetic activity in severe injury

Ang Li [a,b,c,1], Xin Miao [d,a,b,c,1], Zhengzhe Han [a,b,c,1], Junqing Lin [a,b,c], Jinghuan Huang [a,b,c,*], Xianyou Zheng [a,b,c,**]

[a] Department of Orthopedic Surgery, Shanghai Sixth People's Hospital Affiliated to Shanghai Jiao Tong University School of Medicine, No. 600 Yishan Road, Shanghai, 200233, China
[b] National Center for Orthopaedics, No. 600 Yishan Road, Shanghai, 200233, China
[c] Shanghai Institute of Microsurgery on Extremities, Shanghai Sixth People's Hospital Affiliated to Shanghai Jiao Tong University School of Medicine, No. 600 Yishan Road, Shanghai, 200233, China
[d] Department of Orthopaedics, The Third People's Hospital of Chengdu, Sichuan, China

ARTICLE INFO

Keywords:
Bioenergetically-active
Glycerol-based hydrogel
Spinal cord injury
Mitochondrial metabolism

ABSTRACT

Traumatic spinal cord injury (SCI) is a major clinical challenge, imposing a significant burden on both patients and healthcare systems. The complexity of SCI stems from its multifactorial pathogenesis, incorporating a variety of regulating factors. Despite the exploration of mechanisms of SCI pathophysiology and the development of biomedical therapies, current clinical interventions are still limited to surgical interventions and rehabilitative care. This study introduces an approach to protect mitochondria—a pivotal factor in SCI pathogenesis—through the use of poly(glycerol succinate)-based hydrogel. To regulate the process, the PEGylated poly(glycerol succinate) (PPGS), was designed and synthesized via a novel method, combined with recent findings that emphasize the roles of glycerol-based hydrogel in soft tissue regeneration. Building on these, an innovative, bioenergetically-active hydrogel, acrylated PEGylated poly(glycerol succinate) (APPGS), which improves mitochondrial function after injury, targeting SCI treatment, was developed. The evidence, supported by both in vivo and in vitro assays, affirms the therapeutic efficacy of the APPGS hydrogel in SCI contexts. The APPGS hydrogel represents a significant advancement with substantial potential for clinical application in SCI therapy, offering a new avenue for addressing the complex challenges of SCI management.

1. Introduction

Traumatic spinal cord injury (SCI) is a catastrophic event that compromises spinal cord function, with an annual incidence of approximately 23.77 per million people [1]. The management of SCI demands significant healthcare resources and imposes a substantial financial burden on patients, their families, and society [2–4]. Despite half a century of research progress, clinical treatments for SCI are still largely limited to surgical interventions to stabilize and decompress the spinal cord, along with rehabilitative care. Unfortunately, the outcomes of these treatments remain unsatisfactory [5]. The pathological mechanisms underlying the disease involve interconnected events, each exacerbating the other, manifesting as acute axonal degeneration, demyelination, glial scar formation, and cyst formation possibly induced by astrocytes [6]. The vulnerability of spinal cord tissue and the complexity of recovery factors—including neurotrophic factors, interrelated or interlinked multimolecular interactions, and clinical and demographic features—contribute to the limitations of SCI repair [7–9]. These challenges are present throughout the different phases of SCI recovery, which include the acute, subacute, intermediate, and chronic stages. Throughout the phases, energy metabolism is considered a key factor influencing the outcomes of SCI repair, with mitochondria acting

* Corresponding author. Department of Orthopedic Surgery, Shanghai Sixth People's Hospital Affiliated to Shanghai Jiao Tong University School of Medicine, No. 600 Yishan Road, Shanghai, 200233, China.
** Corresponding author. Department of Orthopedic Surgery, Shanghai Sixth People's Hospital Affiliated to Shanghai Jiao Tong University School of Medicine, No. 600 Yishan Road, Shanghai, 200233, China.
E-mail addresses: liang_1@sjtu.edu.cn (A. Li), miaoxin02024924@163.com (X. Miao), hanzhengzhe@sina.com (Z. Han), junqinglinm@163.com (J. Lin), huangjh931@163.com (J. Huang), zhengxianyou@126.com (X. Zheng).
[1] The authors contributed equally to this work.

https://doi.org/10.1016/j.mtbio.2025.101624
Received 21 December 2024; Received in revised form 9 February 2025; Accepted 27 February 2025
Available online 28 February 2025

as a critical regulator [10–12], which can directly affect cellular fitness and cell death, and influence axonal regeneration and functional recovery after SCI [13–15]. Recent therapeutic strategies targeting mitochondria have demonstrated neuroprotective effects. For example, antioxidant therapies have been found to play a vital role in enhancing mitochondrial function in the context of SCI [16]. Additionally, research indicates that regulating mitochondrial homeostasis and neuronal ferroptosis could mitigate the effects of SCI [17]. Furthermore, improving mitochondrial bioenergetics could have significant implications for mitochondrial targeting therapies following central nervous system (CNS) injuries [18]. Therefore, it is crucial to develop methods that provide a better environment for bioenergetics.

Over the past few years, the application of biomaterials in tissue engineering has yielded fruitful research results, becoming a prominent and captivating area of focus [19–21]. Among these, research on hydrogels applied to SCI has provided valuable insights for therapeutic strategies [22,23]. Poly(glycerol sebacate) (PGS) has been proven to be a promising candidate for tissue repair due to its excellent biocompatibility, mechanical properties, and ability to emulate inherent viscoelastic properties. [24–27]. Advances in the synthesis and biomedical applications of PGS have focused on its utility in creating scaffolds for soft tissue engineering [28–30]. These studies highlight the material's softness, robustness, and flexibility, making PGS a compelling option for various biomedical applications. Additionally, its cost-effectiveness compared to other biodegradable elastomers enhances its appeal [26,31]. Combining PGS with chondroitinase ABC (ChABC) has been found to augment nerve regeneration and functional recovery in repairing transected spinal cords in rats [32]. However, pure PGS elastomers cannot form materials with hydrogel properties and therefore cannot be considered glycerol-based hydrogels. In recent years, glycerol-based hydrogels, as a novel class of organo-hydrogels, exhibit easy formability, possess suitable mechanical and physical properties, and their other excellent characteristics make them suitable candidates for drug delivery systems [33,34]. Recent studies have indicated that a bioenergetically active PGS-based multiblock hydrogel (PEPGS) can promote soft tissue recovery by revitalizing mitochondrial metabolism through its central component, glycerol [35]. This finding reveals the potential of such hydrogels in regulating mitochondrial function, which can be a crucial step for tissue regeneration. However, to date, there are no reports of this type of hydrogel being used in the treatment of SCI. To better adapt to SCI scenarios, our research combines recent findings that succinic acid (SA) possesses anti-inflammatory properties and promotes neural repair [36–38]. To further enhance the efficiency and scalability after hydrogel formation, we employed PEGylated poly(glycerol succinate) (PPGS), substituting sebacic acid with succinic acid. This modification made it more suitable for applications in spinal cord tissue engineering. Additionally, the production process was streamlined, thereby making it more suitable for large-scale production. The optimization of this method could facilitate broader application and accessibility of PPGS in biomedical fields. However, pure PPGS cannot form a gel state after dissolving in water; therefore, an acrylation process was introduced to form acrylated PEGylated poly(glycerol succinate) (APPGS), which ensured the curing properties of the hydrogel [39].

Based on the aforementioned approaches, the APPGS hydrogel was prepared for the first time. As an organo-hydrogel, APPGS has potential applications in the biomedical field, such as drug delivery, tissue engineering, and biosensors. This hydrogel exhibits unique mechanical, physical, and chemical properties. By regulating mitochondrial functions, it can significantly enhance the reconnection and regeneration of injured spinal cord tissues, as demonstrated in both in vitro and in vivo studies. This work may provide new insights into the potential role of APPGS in supporting regeneration after SCI, including possible benefits in protecting and restoring intracellular bioenergetics.

2. Materials and methods

2.1. Materials

Glycerol, SA, Polyethylene glycol (PEG, Mn = 1000), p-toluenesulfonic acid monohydrate (PTSA), toluene, p-toluenesulfonyl chloride (TsCl), and dichloromethane (DCM) were purchased from Sigma-Aldrich (USA). Triethylamine (TEA), lithium phenyl-2,4,6-trimethylbenzoylphosphinate (LAP), and acryloyl chloride were procured from Aladdin Chemistry Co., Ltd. (China). Fourier transform infrared (FTIR) spectra were measured by Nicolet 5700, Thermo Fisher Scientific (USA). The proton nuclear magnetic resonance (^{1}H NMR) spectra were recorded on an Avance NMR Spectrometer from Bruker (USA). The cell counting kit 8 was acquired from Dojindo Co. (Japan). The JC-1, MitoTracker Red CMXRos, Calcein-AM/PI, and DAPI were purchased from Beyotime Biotech. Inc. (China). The FITC Annexin V apoptosis detection kit was acquired from BD Biosciences (USA). JCM-7000 scanning electron microscope (SEM) was acquired from JEOL Ltd. (Japan). The antibody was acquired from Cell Signaling Technology, Inc. (USA). The DMi8 was from Leica Microsystems (Germany).

2.2. Synthesis and characterization of APPGS

First, Glycerol monosuccinate was synthesized by reacting equimolar amounts of glycerol and SA dissolved in toluene with PTSA as a catalyst. After removing toluene under reduced pressure, the residue was dissolved in ethyl acetate, filtered, and evaporated to obtain the product. This product was dissolved in DCM with TEA, and TsCl was added to form a tosylate intermediate. PEG in DCM was added to this solution and stirred under nitrogen to form the PPGS precursor. Glycerol was attached to the PEG chain's terminal end, followed by step-growth polymerization. High vacuum and elevated temperature removed by-products. Finally, APPGS was synthesized by modifying the precursor's hydroxyl groups with acryloyl chloride. Characterization using FTIR and ^{1}H NMR confirmed the structures. The APPGS could achieve photo-crosslinking with LAP under a 405 nm blue light source, leading to stable gelation in less than 10 s.

To assess the swelling behavior, the lyophilized hydrogel samples of the same size were positioned in a six-well plate. 2 ml of basic medium was added to cover the samples, followed by incubation at 37 °C. After 24 h, the swelling hydrogels were retrieved with the surface moisture wiped off. After absorbing the excess liquid using filter paper, their weights were determined and the swelling ratio of each was calculated using the following formula:

$$Swelling\ Ratio = \frac{W_t - W_0}{W_0}$$

In the equation, W_t signifies the weight of the hydrogel after swelling, while W_0 denotes the weight of the hydrogel before swelling.

To assess the degradation, the APPGS hydrogel (400 μl), initially preweighed, underwent sterilization via ultraviolet exposure. Subsequently, they were immersed in the preweighed Eppendorf tubes containing basic medium and subjected to incubation in a 5 % CO_2 environment at 37 °C for 28 d. At discrete time intervals, the samples were retrieved and their weights determined. The degradation rate was computed as follows:

$$Degradation\ Rate\ (\%) = \frac{W_0 - W_t}{W_0} \times 100\%$$

In the equation, W_t signifies the final weight of the hydrogel, while W_0 denotes its initial weight.

The morphologies of the hydrogels were assessed using SEM. To prepare the samples, the hydrogels were subjected to a graded ethanol dehydration series. Following dehydration, the samples were lyophilized to fully remove water and prevent structural collapse. After drying,

the samples were sputter-coated with gold to enhance conductivity. The prepared samples were then mounted onto the SEM stage. SEM imaging was conducted by adjusting the accelerating voltage, working distance, and magnification to examine the crosslinked network and pore morphology of the hydrogels.

2.3. Assessment of mechanical properties

The mechanical properties of the hydrogels were measured with a Mars60 rheometer (Haake) equipped with a 25 mm diameter parallel plate geometry at 37 °C. Each hydrogel was gently placed on the center of the rheometer. Frequency sweeps were performed at a constant strain amplitude of 5 % and frequencies of 10 Hz with an applied time of 15min. Uniaxial tensile testing was conducted using the Material Test System (INSTRON 5982), equipped with a 20 N load cell.

2.4. Assessment of biocompatibility and mitochondrial protective effects in vitro

In vitro, the cytotoxicity of APPGS was assessed using the CCK-8 method. Briefly, PC12 cells were cultured in 96-well plates with DMEM and maintained at 37 °C at a density of 10^3 cells per well. For each experimental group, a sample size of three was used (n = 3). Subsequently, the cells were exposed to either 0 or 100 ng/ml LPS, with APPGS, 100 μM SA, or 1 % wt. glycerol, for 3 d. Afterward, the cells in the 96-well plate were treated with CCK-8 and incubated at 37 °C for 1 h at each time point. The absorbance at 450 nm was measured using a multifunctional enzyme marker. Next, the CCK-8 assay results of cells treated with 400 μM tBHP and tBHP with APPGS or 1 % wt. glycerol were compared with untreated cells. The Live/Dead assay was used to assess the status of cells treated with or without tBHP, and with or without APPGS or 1 % wt. glycerol. Calcein-AM was utilized to visualize live cells, while propidium iodide (PI) was employed to identify deceased cells. Calcein AM has an excitation wavelength of 494 nm and an emission wavelength of 517 nm. Conversely, PI exhibits a maximum excitation wavelength of 535 nm and an emission wavelength of 617 nm.

Flow cytometry for apoptosis is also utilized for the detection of effect for PC12 cells treated with or without tBHP, and with or without APPGS or 1 % wt. glycerol. Begin by washing the cells twice using cold PBS, followed by the resuspension of cells in 1 × Binding Buffer at a concentration of 1×10^6 cells/ml. Proceed to transfer 100 μl of this solution into a 5 ml culture tube. Subsequently, introduce 5 μl of FITC Annexin V and 5 μl of PI. Gently vortex the cells, and then allow them to incubate for 15 min at room temperature in darkness. Afterward, add 400 μl of 1 × Binding Buffer to each tube, and finally, conduct the analysis using flow cytometry within 1 h.

For Western blot process of PC12 cells—untreated, treated with tBHP, or treated with tBHP and APPGS—proteins were extracted using radioimmunoprecipitation assay (RIPA) lysis, supplemented with phenylmethylsulfonyl fluoride (PMSF). Protein concentrations were quantified using the BCA Protein Assay Kit (Beyotime, China). These protein samples underwent separation through sodium dodecyl sulfate-polyacrylamide gels (SDS-PAGE) electrophoresis and subsequent transfer onto polyvinylidene fluoride (PVDF) membranes. After blocking, the membranes were incubated overnight at 4 °C with primary antibodies, including anti-Bcl-2 (CST, 3498S, 1:1000, USA), anti-Bax (CST, 14796S, 1:1000, USA), anti-Caspase 3 (CST, 14220S, 1:1000, USA), and anti-β-Actin (CST, 8457, 1:1000, USA). The following day, after incubation with the corresponding secondary antibody, the bands were visualized using enhanced chemiluminescence substrates.

To detect the mitochondrial membrane potential of different groups, the JC-1 assay was used to evaluate the results, with JC-1 monomers exhibiting an excitation wavelength of 514 nm and an emission wavelength of 529 nm, whereas aggregates have an excitation of 585 nm and an emission of 590 nm. MitoTracker Red CMXRos staining assessed the status of intracellular mitochondria. Samples were prepared for confocal microscopy, the platform was adjusted, and images were captured. Additionally, transmission electron microscopy (TEM) presented the imaging of intracellular mitochondria. TEM images were acquired using an HT7800 (Hitachi).

2.5. Evaluation of the functional recovery in vivo

All animal approaches in this study were approved by the Institutional Animal Care and Use Committee (IACUC) of Shanghai Sixth People's Hospital Affiliated to Shanghai Jiao Tong University School of Medicine. Female Sprague-Dawley (SD) rats (250–300 g) were housed under controlled environmental conditions. All surgeries were performed under anesthesia. Rats were anesthetized and exposed to the T9~11 lamina and a laminectomy was performed. Then, a complete surgical transection was performed on the full-transection, PPGS, and APPGS groups. Subsequently, liquids containing PPGS or APPGS were injected into their respective groups. In the APPGS group, a light-curing step was used to form the hydrogel, ensuring its adhesion to both ends of the injury site on the spinal cord. Post-operative care was provided for the rats to prepare for subsequent procedures.

Motor evoked potentials (MEPs) were assessed using the electromyograph and evoked potential equipment. The operation procedure followed the published research [40]. At 4 weeks post-injury (wpi), the rats were anesthetized. The generation of MEPs depended on the stimulation of the corticospinal tract, originating from the motor cortex, achieved through the application of a transcutaneous bipolar electrode positioned on the surface of the skull overlying the motor cortex. Subcutaneous insertion of recording electrodes was performed in the tibialis anterior muscle, and a grounding electrode was subcutaneously placed in the dorsal region.

During the experiments, the locomotion performance of the rats was recorded once a week for up to 8 wpi. Another examiner blinded to the treatment assessed the rats' behavioral performance by The Basso, Beattie, and Bresnahan (BBB) locomotor rating scale [41]. Gait analysis was used to reveal typical sequential footprints after APPGS treatment. The footprints and pressure heat maps were analyzed and compared following previously established methodologies [42]. All quantitative assessments of gait analysis were performed using the VisuGait software by Shanghai XinRuan Information Technology Co.

2.6. Evaluation of the effect on the spinal cord in vivo

At 1 and 8 wpi, animals were euthanized for histological assessment. Following anesthesia of the animals, perfusion was executed using PBS and 4 % paraformaldehyde. The spinal cord tissues were then fixed in 4 % paraformaldehyde overnight, and paraffin-embedded. The samples were sliced into 5 μm sections, and then further stained for histological evaluation. Spinal cord sections at 1 wpi were immunofluorescently labeled with the translocase of the outer mitochondrial membrane 20 (TOM20) and microtubule-associated protein 1A/1B-light chain 3 (LC3) to assess mitochondrial autophagy. Sections at 8 wpi were subjected to H&E staining and immunostaining for myelin basic protein (MBP), indicating remyelination, and growth-associated protein 43 (GAP43), indicative of axonal outgrowth and regeneration. Additionally, sections from both 1 and 8 wpi were immunofluorescently labeled with neuron-specific class III beta-tubulin (Tuj-1), a neuronal marker, and glial fibrillary acidic protein (GFAP), a marker for astrocytes.

At 8 wpi, the liver, kidneys, lungs, and spleen were collected and fixed in 4 % paraformaldehyde. The samples were then dehydrated through a graded ethanol series, embedded in paraffin, sectioned into 5 μm-thick slices, and stained with H&E for histological analysis.

For the transcriptome analysis, rats in both the control group and APPGS group were euthanized and spinal cord tissues were harvested at 1 wpi. Subsequently, RNA sequencing (RNA-seq) was conducted, and the relevant data were analyzed.

2.7. Statistical analysis

In this study, all statistical analyses were performed using the commercial software GraphPad Prism 9, with results expressed as mean ± standard deviation. For comparisons between the two groups, the *t*-test was used. For samples involving three or more groups, one-way analysis of variance (ANOVA) followed by Tukey's post-hoc test was employed. P-value of less than 0.05 is considered statistically significant.

3. Results

3.1. Preparation and characterization of APPGS hydrogel

PPGS undergoes acrylation to form APPGS (Fig. 1A). ^{1}H NMR analyses the structures of PPGS and APPGS polymers (Fig. 1B). The FTIR spectra of PPGS, succinic acid, glycerol, and PEG are presented in Fig. S1. Furthermore, the structural integrity and composition of both APPGS and PPGS were confirmed through FTIR, as shown in Fig. 1C. FTIR analysis particularly highlighted the chemical backbone of the polymers, showcasing a strong ester peak at approximately 1732 cm^{-1} and a broad absorption peak at 1107 cm^{-1}, indicative of hydroxyl groups. A noteworthy observation was the new characteristic absorption peak at ~1652 cm^{-1}, evidencing the successful incorporation of acrylate functional groups into APPGS, which is fundamental to the photo-curing performance [43]. The transition from liquid to solid states of the hydrogel was visually documented, providing a clear before-and-after comparison that showed the rapid solidification capability of the hydrogel (Fig. 1D). SEM imaging provided detailed insights into the internal architecture of both the 20 % and 30 % APPGS hydrogels, as illustrated in Fig. 1E. The SEM images clearly revealed a network of interconnected pores in both samples, underscoring significant differences in pore morphology between the two formulations. The 20 % APPGS hydrogel exhibited a suitable porous structure, with pore sizes that facilitate efficient transport and mechanical stability. In contrast, the 30 % hydrogel presented a denser pore network. Based on these observations, the 20 % APPGS hydrogel was selected for subsequent experiments.

3.2. The mechanical, physical, and chemical properties of APPGS hydrogel

As shown in Fig. 2A, the storage modulus (G') of PGS and APPGS hydrogels was consistently higher than the loss modulus (G"). At the same time, the mechanical properties of the APPGS hydrogel exhibited a significant enhancement to the PGS. Subsequent tensile tests revealed a significant improvement in the mechanical strength of the APPGS hydrogel over its PGS counterpart when prepared under the same conditions (Fig. 2B–D). Interestingly, the swelling ratio of the APPGS hydrogel was found to be not significantly different from that of the PGS (Fig. 2E), indicating similar swelling behavior. The slightly lower swelling property could be attributed to an increased degree of cross-linking [44]. Remarkably, the APPGS hydrogels exhibited a slower rate of degradation over 28 d under simulated physiological conditions compared to PGS (Fig. 2F).

3.3. The regulation of cell activity and anti-apoptotic effects of APPGS in vitro

Combining the performance of APPGS and previous research, we subsequently investigated the effects on PC12 cell lines. The results of

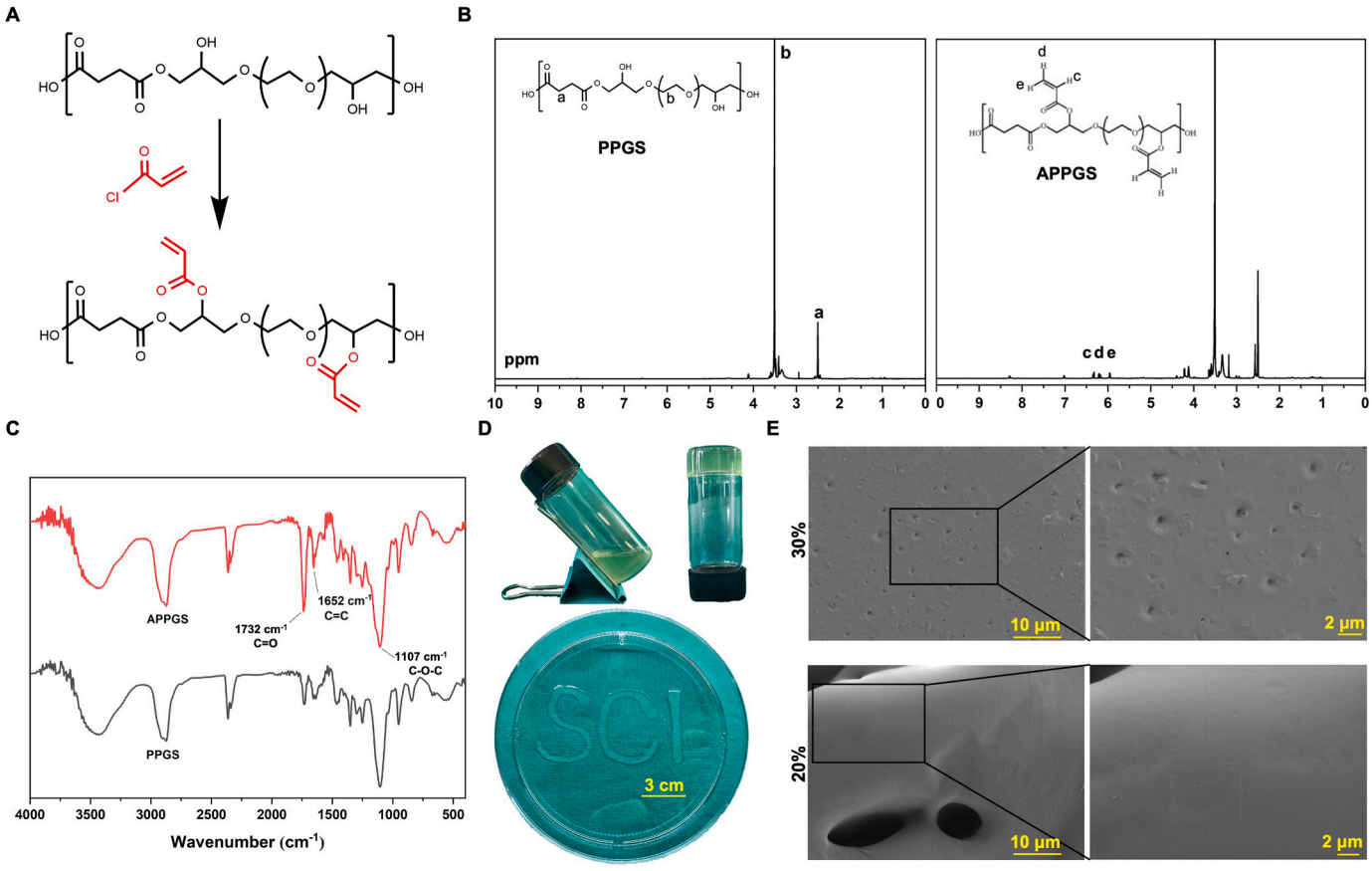

Fig. 1. The fabrication and characteristics of the PPGS and APPGS. A. The process of the PPGS acrylation to form the APPGS. B. The ^{1}H NMR spectrum of the PPGS and APPGS. C. FTIR of the PPGS and APPGS. D. The photographs of the APPGS. E. The SEM images of the 20 % and 30 % APPGS samples.

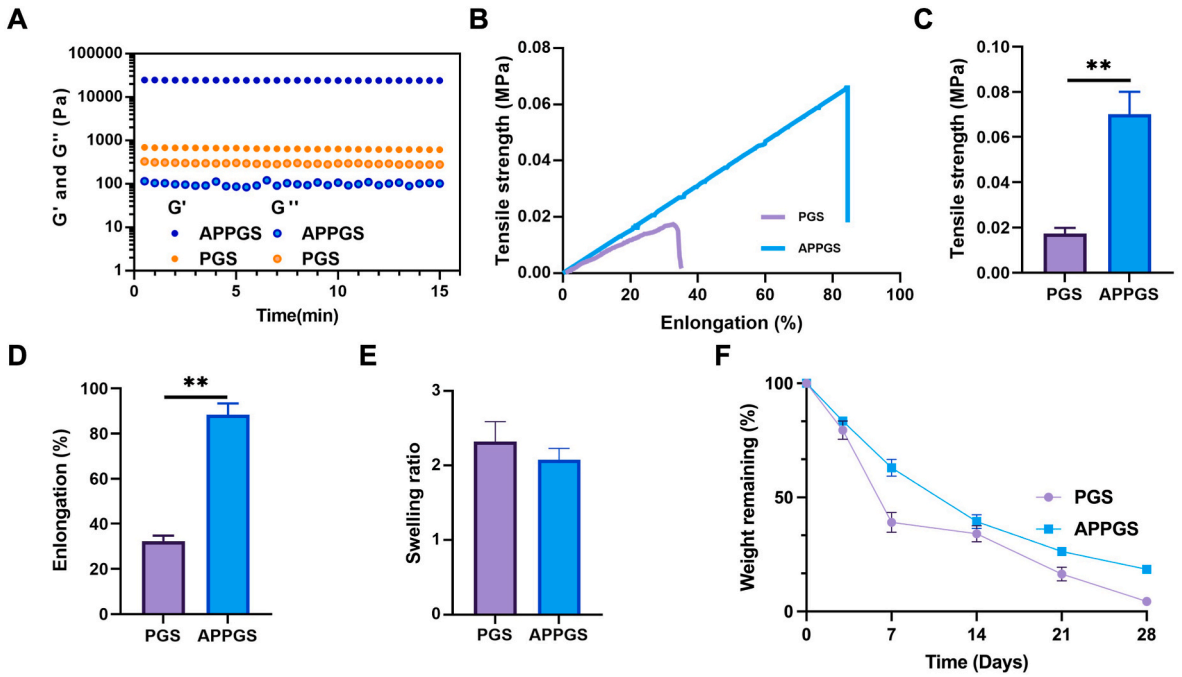

Fig. 2. The mechanical, physical, and chemical properties of APPGS hydrogel. A. The rheology of APPGS and PGS. B. The tensile-elongation curve of APPGS and PGS. C, D. The statistics of the tensile-elongation curve. E. The swelling ratio of APPGS and PGS. F. The degradation of APPGS and PGS in vitro. ** represents the P value < 0.01 between the APPGS group and the PGS group.

CCK8 showed that the cell viability of the APPGS + LPS group was significantly higher than the LPS group (Fig. S2). Further experiments indicated that the APPGS-treated group in an LPS environment showed a significant improvement compared to groups treated with SA or glycerol (Fig. S3). Live/Dead assay showed that the dead cell ratio of the glycerol group in the tBHP environment was higher than the APPGS group (Fig. 3A). The cell viability of the group treated with APPGS in the tBHP environment was significantly higher than that of the groups with tBHP alone or tBHP with glycerol (Fig. 3B). The flow cytometry showed that apoptosis cell proportion treated with the APPGS group was significantly lower than the glycerol group in the tBHP environment (Fig. 3C and D). The Western blot results provided additional insights into the mechanisms by which APPGS may exert protective effects against cell apoptosis (Fig. 3E and F). The analysis revealed alterations in the expression of apoptosis-related proteins, specifically an upregulation of anti-apoptotic proteins and a downregulation of pro-apoptotic proteins.

3.4. The anti-mitochondrial apoptosis capability of APPGS in vitro

The TEM results revealed that mitochondria in the APPGS-treated cells in a tBHP environment exhibited a morphology characterized by less swollen and a more defined cristae structure, indicative of healthier mitochondrial conditions (Fig. 4A). Furthermore, the application of APPGS resulted in mitochondria that were not only structurally preserved but also functionally enhanced. This was evidenced by Mito-Tracker Red CMXRos staining, which demonstrated increased mitochondrial activity in the APPGS group compared to the groups with tBHP alone or tBHP with glycerol (Fig. 4C and D). JC-1 assay results showed that the green fluorescence intensity of the groups with tBHP alone or tBHP with glycerol in a tBHP environment was higher than the APPGS or control group, thereby the proportion of normal mitochondrial membrane potential was maintained with APPGS (Fig. 4E). Consequently, this suggests that mitochondrial function with APPGS treatment more closely resembles that of normal cells. Furthermore, flow cytometry results in Fig. 4F and G showed a similar trend in cell proportions in the LR quadrant, demonstrating the protective effects of APPGS on mitochondria [45]. The method used to co-culture PC12 cells with the APPGS hydrogel is shown in Fig. 4B.

3.5. The impact of APPGS on the locomotor function recovery in vivo

The time points and treatment regimen were as indicated in Fig. 5A. The BBB locomotor rating scale suggested a significant improvement in the APPGS-treated group (Fig. 5B). Further corroborating the BBB score findings, the MEP analysis offered additional evidence of neurological recovery. Both the amplitude and latency of MEPs in the APPGS group were indicative of improved neural conduction and muscle response capabilities (Fig. 5C–E). Moreover, the gait analysis of the APPGS group revealed a more regular stepping pattern when compared to the control group, pointing towards a recovery of coordinated motor activity [46] (Fig. 5F, Fig. S4). The analysis of footprints, an objective measure of gait quality, showed that the APPGS group's stepping pattern was not only more consistent but also exhibited footprint pressure values that approached those of normal, uninjured subjects (Fig. 5G–J). This normalization in gait and pressure distribution highlights the significant impact of APPGS on restoring locomotor function.

3.6. The tissue recovery situation after using APPGS

8 wpi after the application of APPGS, H&E staining was conducted to assess the pathological changes following SCI (Fig. 6A). The results showed that neurons in the sham operation group appeared normal, with intact nuclei, along with clear nucleoli. In contrast, the SCI control and APPGS treated groups exhibited neuronal swelling, shrunken neurons with darkly stained, condensed nuclei, and a significant loss and damage of both neuronal and glial cells. Additionally, the tissue structure appeared disordered and irregularly arranged. However, APPGS treatment led to noticeable improvements in the pathological changes, as the cavity size in the APPGS-treated group was reduced compared to the control group. The analysis of GFAP expression levels revealed a noteworthy distinction between the control, PPGS-treated groups, and the APPGS-treated group at both 1 and 8 wpi, as demonstrated in Fig. 6B–D. Specifically, the GFAP levels in the control and PPGS groups were observed to be higher compared to those in the APPGS group.

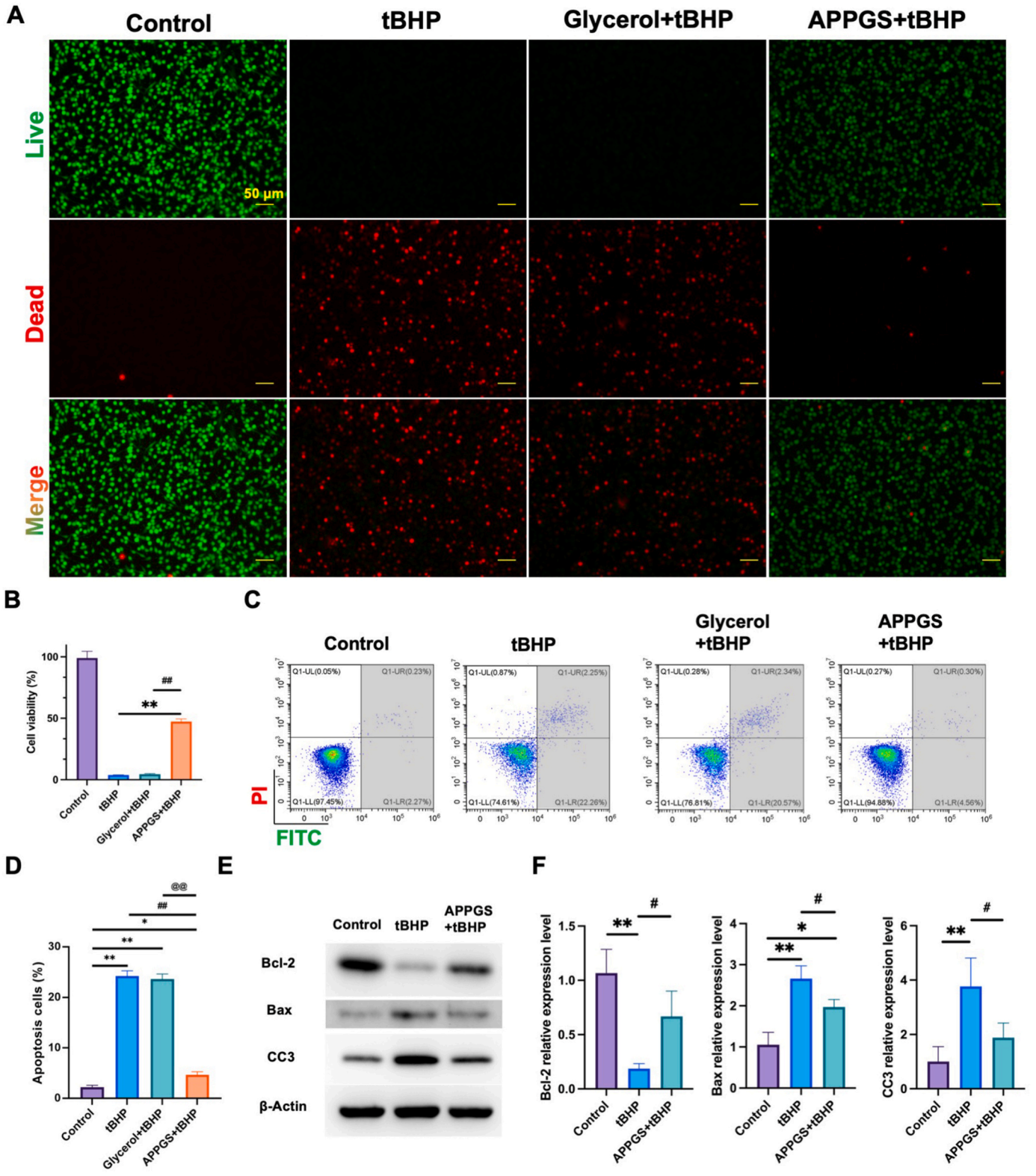

Fig. 3. In vitro experiments on the cell activity and anti-apoptotic effects of APPGS. A. The Live/Dead assay results. B. The cell viability assay. ** represents the P value < 0.01 between the tBHP group and the designated group. ##represents the P value < 0.01 between the glycerol + tBHP group and the designated group. C. The level of apoptosis was detected by flow cytometry. D. The flow cytometry showed the apoptotic ratio in different groups. * represents the P value < 0.05 between the control group and the designated group. ** represents the P value < 0.01 between the control group and the designated group. ##represents the P value < 0.01 between the tBHP group and the designated group. @@ represents the P value < 0.01 between the glycerol + tBHP group and the designated group. E. Protein expression results of Bcl-2, Bax, and CC3 were determined by Western blot. F. The statistics of Western blot results. * represents the P value < 0.05 between the control group and the designated group. ** represents the P value < 0.01 between the control group and the designated group. # represents the P value < 0.05 between the tBHP group and the designated group.

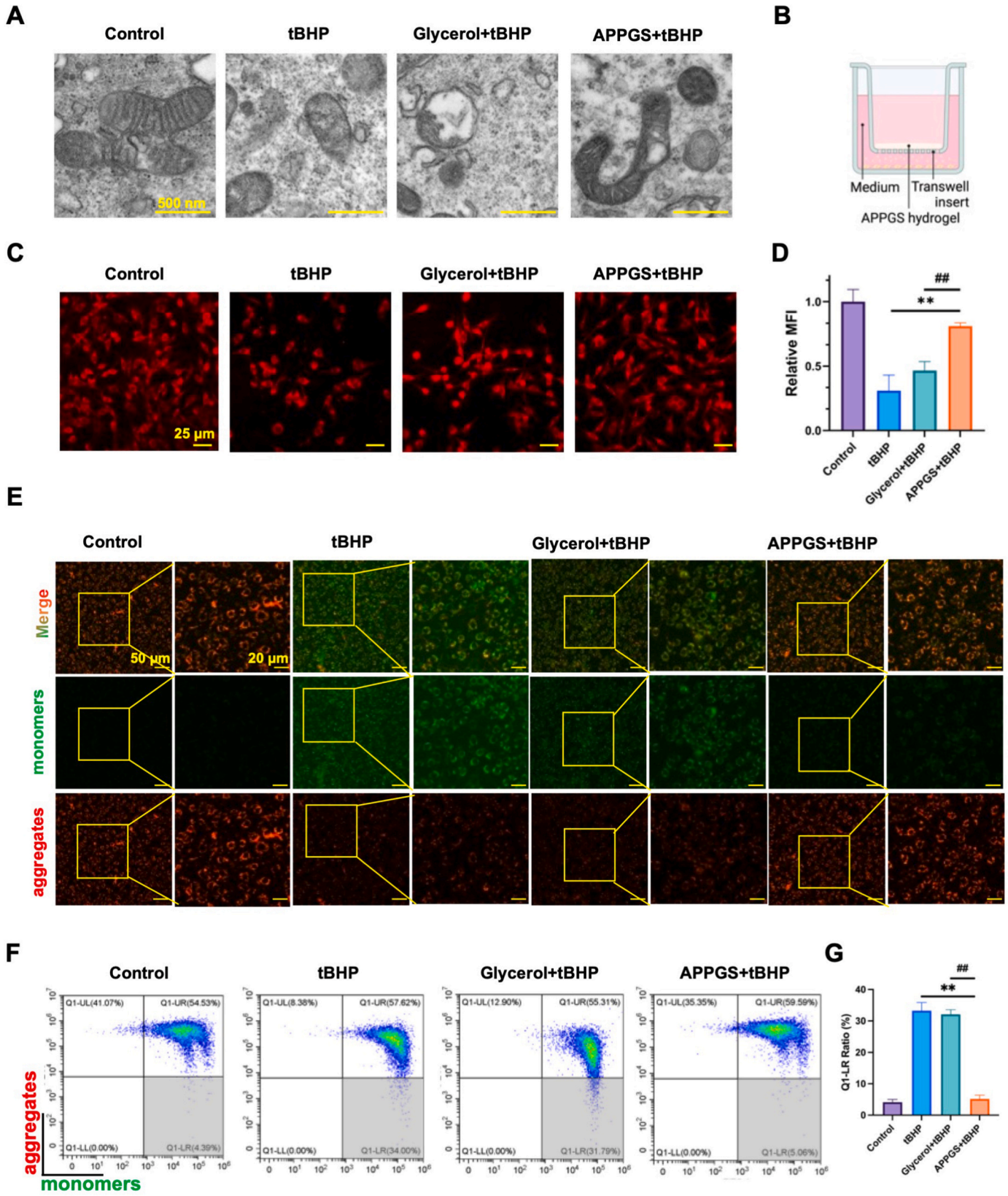

Fig. 4. The mitochondria morphology and function in different groups. A. The TEM of mitochondria. B. The scheme of the PC12 cells co-cultured with APPGS hydrogel in the transwell. C. The MitoTracker Red CMXRos results of the PC12 cells. D. Quantitative analysis of MitoTracker Red CMXRos for different groups. E. The results of the JC-1 assay were observed with the fluorescence microscope. F. The results of flow cytometry of JC-1. G. Quantitative analysis of Q1-LR in flow cytometry for different groups. (For interpretation of the references to colour in this figure legend, the reader is referred to the Web version of this article.)

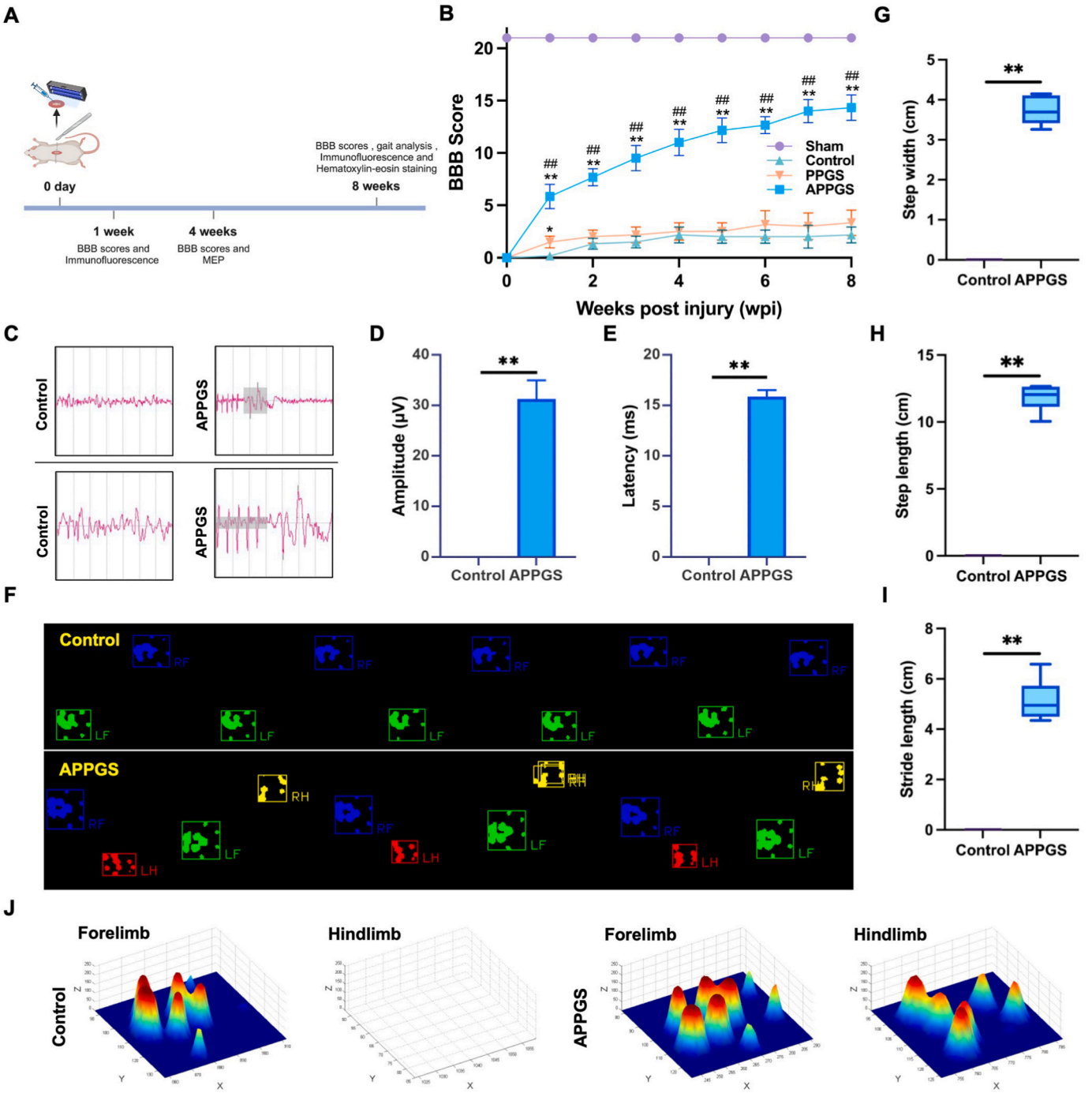

Fig. 5. In vivo locomotor function recovery following APPGS hydrogel treatment. A. Schematic diagram of the in vivo experimental procedures. B. BBB score results for the different treatment groups. C. MEP waveforms of the different groups. D. Quantitative analysis of MEP amplitude. E. Quantitative analysis of MEP latency. F. Gait analysis illustrating functional recovery in the in vivo experiments (blue indicates the right forelimb, green indicates the left forelimb, yellow indicates the right hindlimb, and red indicates the left hindlimb). G. Quantitative analysis of step width in each group. H. Quantitative analysis of step length in each group. I. Quantitative analysis of stride length in each group. J. Footprint pressure heatmaps. * represents the P value < 0.05 between the control group and the PPGS or APPGS group. ** represents the P value < 0.01 between the control group and the PPGS or APPGS group. ## represents the P value < 0.01 between the PPGS group and the APPGS group. (For interpretation of the references to colour in this figure legend, the reader is referred to the Web version of this article.)

Additionally, the expression of Tuj-1, a marker for neuronal differentiation and axonal regeneration, showed significant improvement in the APPGS-treated group compared to that of the control and PPGS groups (Fig. 6E–G). More compelling, however, was the observation of MBP and GAP43 expression in the APPGS group (Fig. 6H and I). The fluorescence intensity was significantly higher than that in both the control and PPGS groups, as shown in Fig. 6J and K.

3.7. Regulation of in vivo mitophagy by APPGS

At 1 wpi, the in vivo results indicate that following APPGS treatment, cellular TOM20 and LC3 expression levels in spinal cord tissue were significantly higher compared to both the PPGS and control groups (Fig. 7A–C).

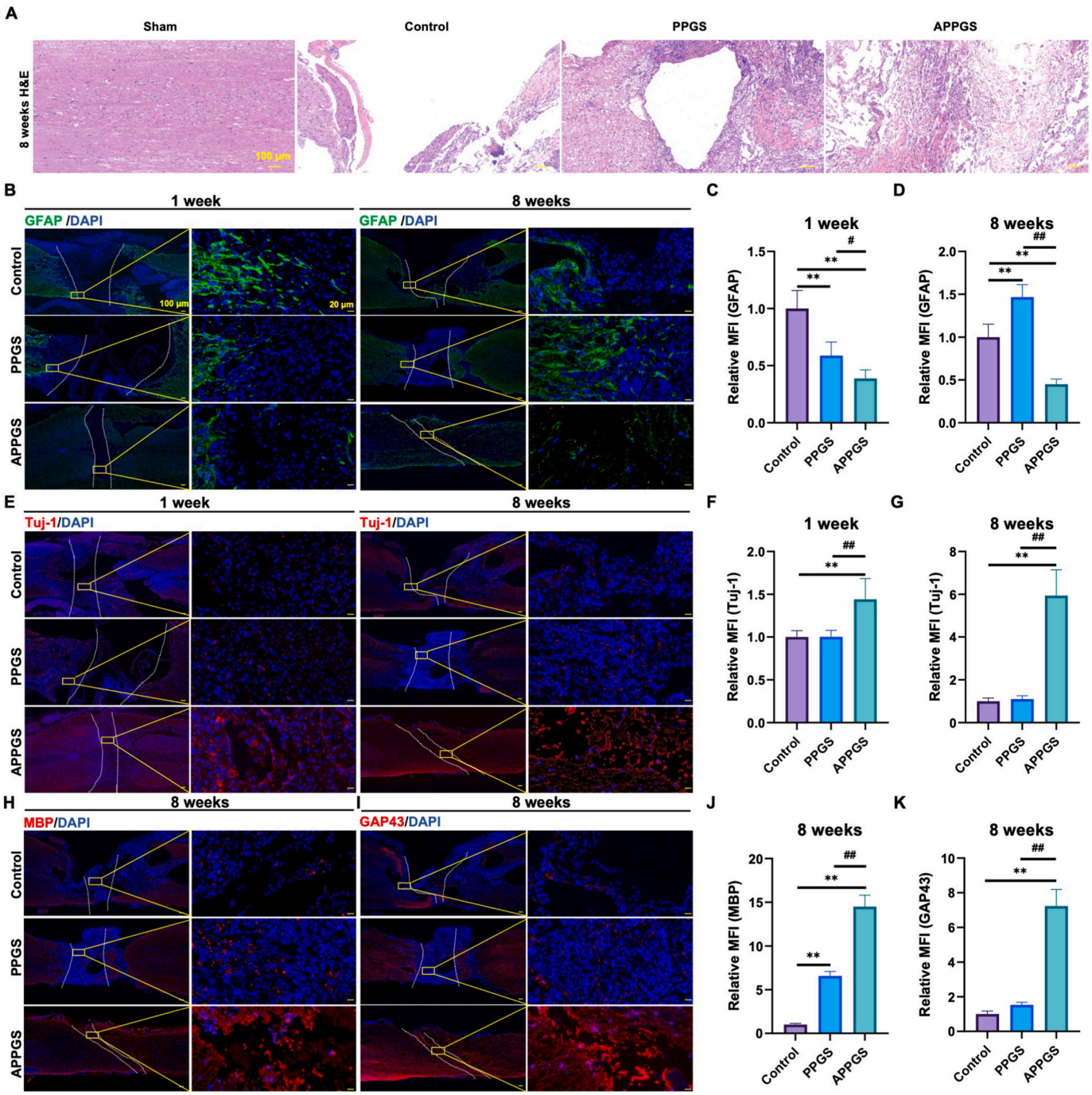

Fig. 6. The results of the spinal cord tissue recovery in vivo treated with APPGS hydrogel. A. H&E staining sections of different groups. B. The GFAP expression was revealed of the injured site in different groups at 1 and 8 wpi. C. The relative MFI of GFAP in different groups at 1 wpi. D. The relative MFI of GFAP in different groups at 8 wpi. E. The Tuj-1 expression was revealed of the injured site in different groups at 1 and 8 wpi. F. The relative MFI of Tuj-1 in different groups at 1 wpi. G. The relative MFI of Tuj-1 in different groups at 8 wpi. H. The MBP expression was revealed of the injured site in different groups at 8 wpi. I. The GAP43 expression was revealed of the injured site in different groups at 8 wpi. J. The relative MFI of MBP in different groups at 8 wpi. K. The relative MFI of GAP43 in different groups at 8 wpi. ** represents the P value < 0.01 between the control group and the designated group. #represents the P value < 0.05 between the PPGS group and the APPGS group. ##represents the P value < 0.01 between the PPGS group and the APPGS group.

3.8. Biotoxicity assessment in vivo after APPGS application

H&E staining of the vital organs from rats treated with APPGS revealed no inflammatory reactions, indicating that the hydrogel is biocompatible in vivo and thus holds promise for clinical applications (Fig. 8).

3.9. Spinal cord tissue transcriptomic sequencing results after APPGS application

To unravel the intricate cellular mechanisms of APPGS accelerating SCI repair, we performed RNA-seq analysis in control and APPGS-treated groups derived from samples at 1 wpi. Comparing the APPGS group with the control group, a volcano plot showed the differentially expressed genes, including down-regulated and up-regulated genes

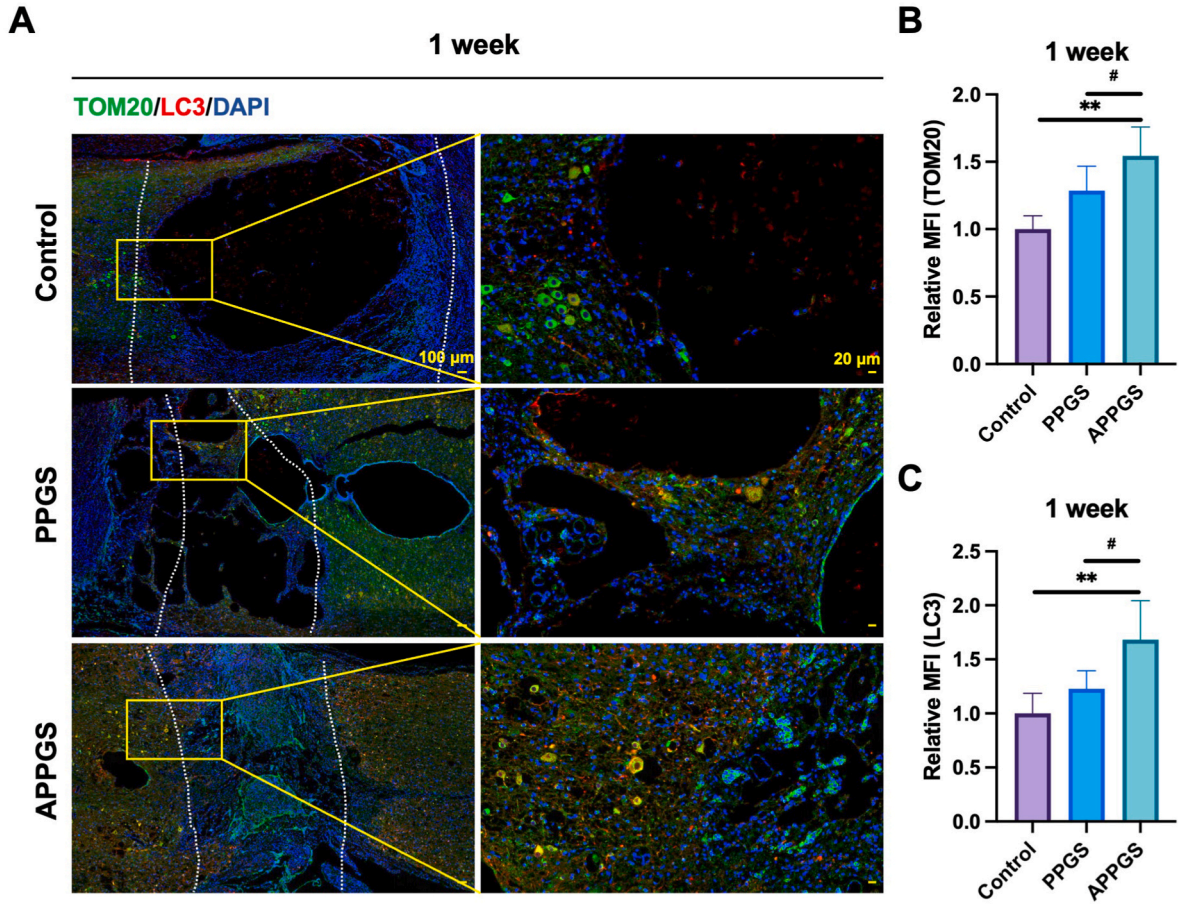

Fig. 7. In vivo immunofluorescence analysis of mitophagy. A. Representative images of TOM20 and LC3 expression at the injury site in each experimental group at 1 wpi. B. Relative MFI of TOM20 in the various groups at 1 wpi. C. Relative MFI of LC3 in the different groups at 1 wpi. ** indicates $P < 0.01$ compared to the control group, and # indicates $P < 0.05$ compared to the PPGS group.

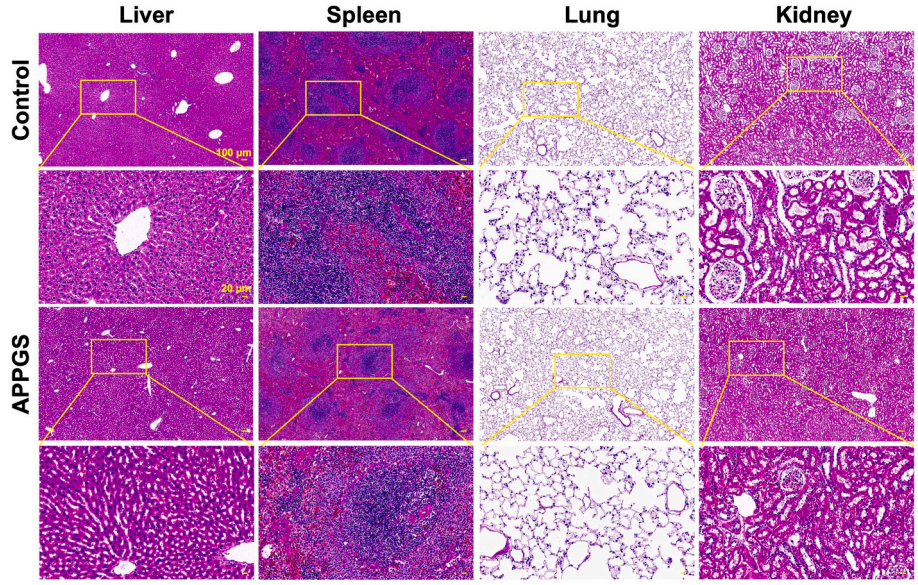

Fig. 8. Biotoxicity evaluation on tissue sections of vital organs. At 8 wpi, H&E staining was performed on vital organs of rats treated with APPGS to assess any significant inflammatory response.

(Fig. 9A). Gene Ontology (GO) with Kyoto Encyclopedia of Genes and Genomes (KEGG) analysis revealed the pathways related to cell apoptosis that are involved in the effects of APPGS (Fig. 9B–E). These findings revealed the p53 signaling pathway as a potential factor intertwined with these changes.

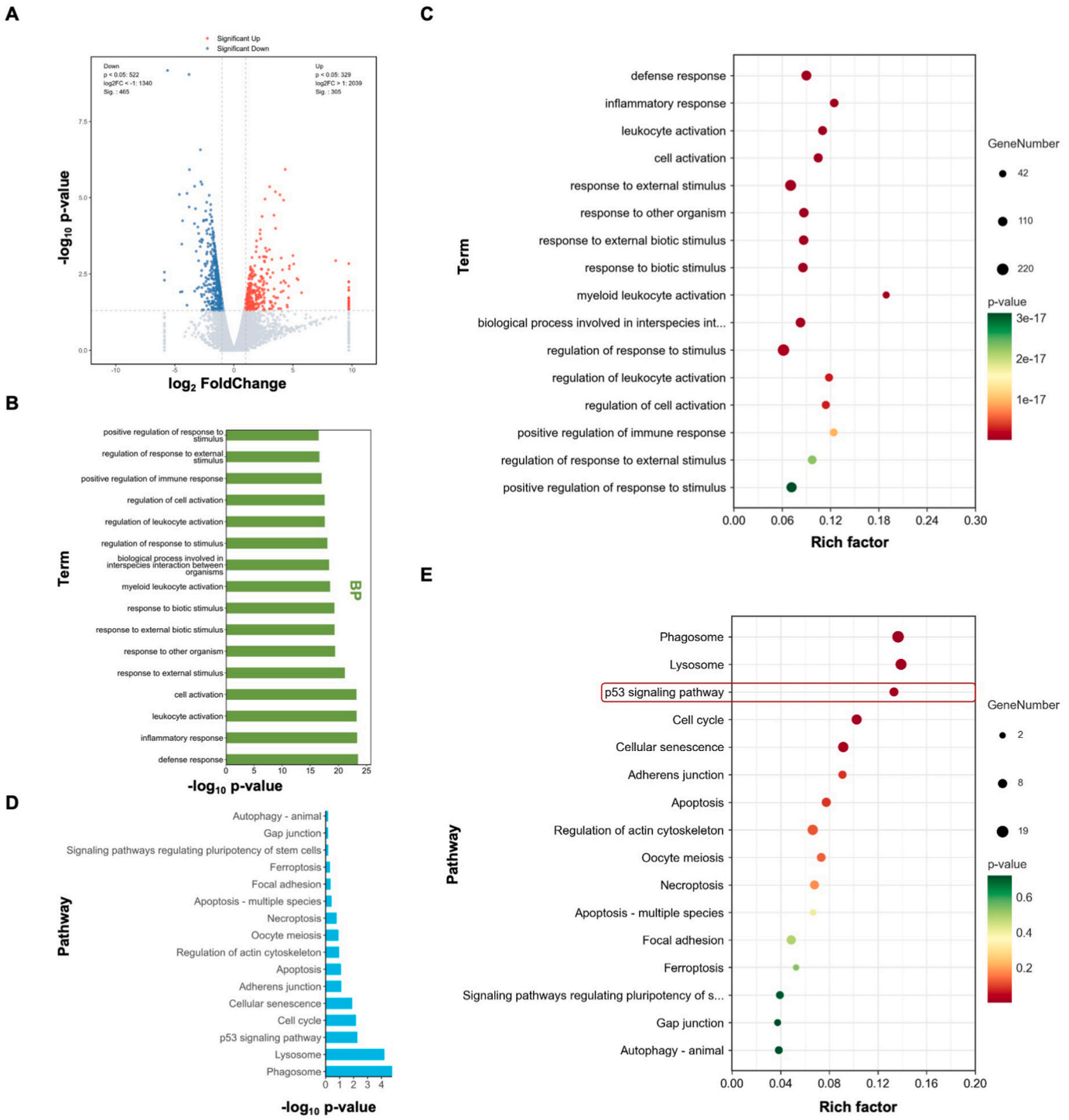

Fig. 9. Transcriptome analysis of the APPGS-treated group compared with the control group. A. Volcano plot of differentially expressed genes (DEGs) between the control and APPGS-treated groups. Red dots denote significantly upregulated genes, blue dots denote significantly downregulated genes, and gray dots denote genes without significant changes. B. Bar chart showing Gene Ontology (GO) enrichment analysis of Biological Process (BP) terms for the identified DEGs. C. Bubble chart illustrating GO enrichment of BP terms for the DEGs. D. Bar chart of KEGG pathway enrichment analysis. E. Bubble chart of KEGG pathway enrichment. (For interpretation of the references to colour in this figure legend, the reader is referred to the Web version of this article.)

4. Discussion

SCI may permanently affect spinal cord function, causing familial and socioeconomic burdens. The pathology of SCI is relatively complex, but mitochondrial dysfunction impacts all stages of the disease [12,47]. Building upon previous studies where glycerol-based hydrogels regulate tissue mitochondria to promote tissue regeneration [35], PPGS was developed to regulate mitochondria after SCI to promote spinal cord tissue regeneration. ^{1}H NMR and FTIR results confirmed the successful synthesis of PPGS. To achieve better curing into hydrogels for application in tissue engineering, an acrylation process was employed to synthesize APPGS. The SEM results indicated that the 20 % APPGS hydrogel was more suitable for biomedical applications. It exhibited an optimized porous structure for future experimentation and potential clinical use. In

recent years, PGS-based biomaterials have received tremendous attention in fields such as cardiovascular [48], neural [49], and cartilage tissue engineering [50,51]. Notably, a recent study has demonstrated that poly(glycerol sebacate)-based multiblock hydrogels can effectively revitalize mitochondrial metabolism in both in vitro and in vivo experiments [35]. The observed enhancement in mechanical properties indicates that, compared to PGS, APPGS is a more robust and durable option for biomedical applications. The increased strength of APPGS hydrogel suggests its suitability for environments requiring substantial mechanical support. Meanwhile, the appropriate degradation of the APPGS hydrogel in a simulated physiological environment demonstrates its compatibility with biological environments, allowing it to function effectively and promote seamless tissue growth [52]. Compared to existing hydrogel systems, the APPGS hydrogel offers several advantages. It exhibits excellent biocompatibility, showing no cytotoxicity, good in vitro degradability, and outstanding swelling properties. Additionally, its mechanical properties are superior; the rheological performance and elongation at break significantly exceed those of current PGS. The APPGS hydrogel can be synthesized industrially and used on a large scale. Compared to other expensive materials that incorporate bioactive factors, it is easier to store, transport, and use. Its manufacturing process can be implemented in standard-sized factories within industrial zones. As is well known, PGS-type materials, due to their excellent properties, can achieve outstanding drug-loading effects and can be more easily grafted and chemically modified. In vitro experiments found that APPGS can increase the survival rate of PC12 cells under tBHP conditions and reduce apoptosis. The shift in protein expression patterns suggests that APPGS could modulate the cellular apoptotic machinery, thereby enhancing cell survival under conditions that would typically induce cell death.

TEM analysis of mitochondria in the APPGS-treated group provided compelling insights into the protective effects of APPGS on mitochondrial structure and function. The results suggested that APPGS played a critical role in preserving the integrity of mitochondrial architecture, thereby contributing to cellular resilience against stressors [53]. Subsequent experiments found that increased mitochondrial activity is proof of the efficacy of APPGS in promoting mitochondrial function and inhibiting apoptosis, which is essential for energy production and cellular health. In vivo experiments demonstrated that the observed improvements in locomotor function, neural conduction, and gait regularity collectively affirm the efficacy of APPGS in promoting neurological and functional recovery. These results suggest that APPGS treatment may contribute to the restoration of neural pathways essential for motor function. The synergy of these findings, from the BBB scores and MEP results to the detailed gait analysis, paints a comprehensive picture of the therapeutic potential of APPGS in enhancing motor recovery after SCI [54]. In vivo immunofluorescence analyses demonstrated that APPGS treatment significantly enhanced mitophagy. Further results indicate that a decrease in GFAP expression within the APPGS group suggests a less astrocytic response, which could be indicative of the level of glial reaction to injury being down-regulated [55]. The increase in Tuj-1 expression levels suggests that APPGS may enhance certain aspects of the neural environment post-injury and affect neuronal differentiation. MBP is a critical component of the myelin sheath, and its increased expression in the APPGS group suggests an enhanced process of myelination or remyelination. GAP43 is widely regarded as an intrinsic determinant of neural growth and regeneration, and its elevated levels in the APPGS group point towards an augmented capacity for axonal sprouting and neural repair. Due to the hostile environment at the injured site, biomaterials are needed to bridge the tissues and create a regenerative environment [56]. These findings highlight the multifaceted impact of APPGS treatment on the neural tissue post-SCI. The changed Tuj-1 expression indicates that neuronal differentiation was affected by APPGS treatment, while the significant increase in MBP and GAP43 expression underscores the potent regenerative and myelinating capabilities conferred by APPGS treatment [57–59]. Previous studies have shown that PEG can exert neuroprotective effects by reducing oxidative stress and mitigating mitochondrial dysfunction [60]. This study showed that when PEG is combined with glycerol and succinic acid, the resulting APPGS formulation can effectively promote spinal cord tissue repair and regulate mitochondrial function after SCI.

P53 signaling pathway is renowned for its critical role in modulating mitochondrial apoptosis. This study reveals a deep-seated link between APPGS application and the inhibition of mitochondrial apoptosis and the enhancement of bioenergetics [61–65]. Together, these results delineate a complex picture of the neural repair mechanisms activated by APPGS, illustrating its potential as a therapeutic agent in enhancing neural regeneration and recovery following SCI. While the study demonstrates the hydrogel's effectiveness in promoting mitochondrial function and tissue repair, future research should further explore the mechanisms of the hydrogel.

5. Conclusion

The APPGS hydrogel represents a significant breakthrough in the treatment of SCI by offering a novel approach that promotes bioenergetics. The APPGS hydrogel can be synthesized on an industrial scale and used extensively. Compared to other expensive materials that incorporate bioactive factors, it is easier to store, transport, and utilize. This strategy not only addresses the immediate aftermath of SCI but also lays the groundwork for long-term recovery and tissue repair. Both in vivo and in vitro results demonstrate that APPGS not only mitigates cell apoptosis but also fosters an environment conducive to the regeneration and repair of damaged spinal cord tissues. By pursuing future research directions, APPGS has the potential to revolutionize SCI therapy, offering new hope for patients and advancing the field of regenerative medicine.

CRediT authorship contribution statement

Ang Li: Writing – original draft, Resources, Methodology, Investigation, Conceptualization. **Xin Miao:** Software, Investigation, Formal analysis, Data curation. **Zhengzhe Han:** Visualization, Methodology, Investigation, Data curation. **Junqing Lin:** Validation, Project administration. **Jinghuan Huang:** Writing – review & editing, Supervision, Resources, Project administration, Conceptualization. **Xianyou Zheng:** Writing – review & editing, Supervision, Resources, Project administration, Funding acquisition, Conceptualization.

Declaration of competing interest

The authors declare that they have no known competing financial interests or personal relationships that could have appeared to influence the work reported in this paper.

Acknowledgements

The authors would like to express their gratitude for the financial support from the National Natural Science Foundation of China (No. 82172421, 82372388). The authors thank Haobo Technology Company for their assistance in this research.

Appendix A. Supplementary data

Supplementary data to this article can be found online at https://doi.org/10.1016/j.mtbio.2025.101624.

Data availability

Data will be made available on request.

References

[1] Y. Lu, Z. Shang, W. Zhang, M. Pang, X. Hu, Y. Dai, R. Shen, Y. Wu, C. Liu, T. Luo, X. Wang, B. Liu, L. Zhang, L. Rong, Global incidence and characteristics of spinal cord injury since 2000–2021: a systematic review and meta-analysis, BMC Med. 22 (2024) 1–13, https://doi.org/10.1186/S12916-024-03514-9/FIGURES/7.

[2] C.S. Ahuja, J.R. Wilson, S. Nori, M.R.N. Kotter, C. Druschel, A. Curt, M.G. Fehlings, Traumatic spinal cord injury, Nat. Rev. Dis. Primers 3 (1 3) (2017) 1–21, https://doi.org/10.1038/nrdp.2017.18, 2017.

[3] A. Singh, L. Tetreault, S. Kalsi-Ryan, A. Nouri, M.G. Fehlings, S. Kalsi, R. Aria, N. Michael, G. Fehlings, Global Prevalence and incidence of traumatic spinal cord injury, Clin. Epidemiol. 6 (2014) 309–331, https://doi.org/10.2147/CLEP.S68889.

[4] B.B. Lee, R.A. Cripps, M. Fitzharris, P.C. Wing, The global map for traumatic spinal cord injury epidemiology: update 2011, global incidence rate, Spinal Cord 52 (2 52) (2013) 110–116, https://doi.org/10.1038/sc.2012.158, 2013.

[5] A.F. Cristante, T.E.P. de Barros Filho, R.M. Marcon, O.B. Letaif, I.D. da Rocha, Therapeutic approaches for spinal cord injury, Clinics 67 (2012) 1219–1224, https://doi.org/10.6061/CLINICS/2012(10)16.

[6] A. Anjum, M.D. Yazid, M.F. Daud, J. Idris, A.M. Hwei Ng, A.S. Naicker, O. H. Rashidah Ismail, R.K.A. Kumar, Y. Lokanathan, Spinal cord injury: pathophysiology, multimolecular interactions, and underlying recovery mechanisms, Int. J. Mol. Sci. 21 (2020) 7533, https://doi.org/10.3390/IJMS21207533, 7533 21 (2020).

[7] H. Beverungen, S.C. Klaszky, M. Klaszky, M.P. Côté, Rehabilitation decreases Spasticity by restoring chloride homeostasis through the brain-derived neurotrophic factor-KCC2 pathway after spinal cord injury, J. Neurotrauma 37 (2020) 846–859, https://doi.org/10.1089/NEU.2019.6526.

[8] X. Miao, J. Lin, A. Li, T. Gao, T. Liu, J. Shen, Y. Sun, J. Wei, B. Bao, X. Zheng, AAV-mediated VEGFA overexpression promotes angiogenesis and recovery of locomotor function following spinal cord injury via PI3K/Akt signaling, Exp. Neurol. (2024) 114739, https://doi.org/10.1016/J.EXPNEUROL.2024.114739.

[9] G. Scivoletto, F. Tamburella, L. Laurenza, M. Torre, M. Molinari, Who is going to walk? A review of the factors influencing walking recovery after spinal cord injury, Front. Hum. Neurosci. 8 (2014) 76963, https://doi.org/10.3389/FNHUM.2014.00141/BIBTEX.

[10] A.G. Rabchevsky, F.M. Michael, S.P. Patel, Mitochondria focused neurotherapeutics for spinal cord injury, Exp. Neurol. 330 (2020) 113332, https://doi.org/10.1016/J.EXPNEUROL.2020.113332.

[11] A.N. Stewart, K.E. McFarlane, H.J. Vekaria, W.M. Bailey, S.A. Slone, L. A. Tranthem, B. Zhang, S.P. Patel, P.G. Sullivan, J.C. Gensel, Mitochondria exert age-divergent effects on recovery from spinal cord injury, Exp. Neurol. 337 (2021) 113597, https://doi.org/10.1016/J.EXPNEUROL.2021.113597.

[12] P.G. Slater, M.E. Domínguez-Romero, M. Villarreal, V. Eisner, J. Larraín, Mitochondrial function in spinal cord injury and regeneration, Cell. Mol. Life Sci. 79 (5 79) (2022) 1–24, https://doi.org/10.1007/S00018-022-04261-X, 2022.

[13] E. Kummer, N. Ban, Mechanisms and regulation of protein synthesis in mitochondria, Nat. Rev. Mol. Cell Biol. 22 (5 22) (2021) 307–325, https://doi.org/10.1038/s41580-021-00332-2, 2021.

[14] F.J. Bock, S.W.G. Tait, Mitochondria as multifaceted regulators of cell death, Nat. Rev. Mol. Cell Biol. 21 (2020) 85–100, https://doi.org/10.1038/s41580-019-0173-8.

[15] Q. Han, Y. Xie, J.D. Ordaz, A.J. Huh, N. Huang, W. Wu, N. Liu, K.A. Chamberlain, Z.H. Sheng, X.M. Xu, Restoring cellular Energetics promotes axonal regeneration and functional recovery after spinal cord injury, Cell Metab. 31 (2020) 623–641.e8, https://doi.org/10.1016/J.CMET.2020.02.002/ATTACHMENT/4C60532C-B142-4F3C-A8EA-459DAA78C692/MMC2.PDF.

[16] D. Chen, L. Zhou, G. Chen, T. Lin, J. Lin, X. Zhao, W. Li, S. Guo, R. Wu, Z. Wang, W. Liu, FUNDC1-induced mitophagy protects spinal cord neurons against ischemic injury, Cell Death Discovery 10 (1 10) (2024) 1–12, https://doi.org/10.1038/s41420-023-01780-9, 2024.

[17] S. Yao, M. Pang, Y. Wang, X. Wang, Y. Lin, Y. Lv, Z. Xie, J. Hou, C. Du, Y. Qiu, Y. Guan, B. Liu, J. Wang, A.P. Xiang, L. Rong, Mesenchymal stem cell attenuates spinal cord injury by inhibiting mitochondrial quality control-associated neuronal ferroptosis, Redox Biol. 67 (2023), https://doi.org/10.1016/J.REDOX.2023.102871.

[18] G.V. Velmurugan, W.B. Hubbard, P. Prajapati, H.J. Vekaria, S.P. Patel, A. G. Rabchevsky, P.G. Sullivan, LRP1 Deficiency promotes Mitostasis in response to oxidative stress: implications for mitochondrial targeting after traumatic brain injury, Cells 12 (2023), https://doi.org/10.3390/CELLS12101445.

[19] H. Zhou, Z. Li, S. Jing, B. Wang, Z. Ye, W. Xiong, Y. Liu, Y. Liu, C. Xu, T. Kumeria, Y. He, Q. Ye, Repair spinal cord injury with a versatile anti-oxidant and neural regenerative nanoplatform, J Nanobiotechnology 22 (2024) 1–24, https://doi.org/10.1186/S12951-024-02610-5/FIGURES/8.

[20] J. Lin, W. Hu, T. Gao, B. Bao, X. Li, T. Huang, Y. Sun, J. Shen, H. Xu, K. Zhu, H. Zhu, Y. Yang, X. Zheng, ε-Poly-l-lysine as an efficient cartilage penetrating and residing drug carrier with high intraarticular injection safety for treating osteoarthritis, Chem. Eng. J. 430 (2022) 133018, https://doi.org/10.1016/J.CEJ.2021.133018.

[21] Z. Han, A. Li, Z. Xue, S. bing Guan, G. Yin, X. Zheng, Eugenol-loaded polyurethane gelatin dressing for efficient angiogenesis and antibacterial effects in refractory diabetic wound defect healing, Int. J. Biol. Macromol. 271 (2024), https://doi.org/10.1016/J.IJBIOMAC.2024.132619.

[22] H. Zhou, S. Jing, W. Xiong, Y. Zhu, X. Duan, R. Li, Y. Peng, T. Kumeria, Y. He, Q. Ye, Metal-organic framework materials promote neural differentiation of dental pulp stem cells in spinal cord injury, J Nanobiotechnology 21 (2023) 1–18, https://doi.org/10.1186/S12951-023-02001-2/FIGURES/8.

[23] A.A. Albashari, Y. He, Y. Luo, X. Duan, J. Ali, M. Li, D. Fu, Y. Xiang, Y. Peng, S. Li, L. Luo, X. Zan, T. Kumeria, Q. Ye, Local spinal cord injury treatment using a dental pulp stem cell Encapsulated H2S Releasing multifunctional injectable hydrogel, Adv Healthc Mater 13 (2024) 2302286, https://doi.org/10.1002/ADHM.202302286.

[24] R. Rai, M. Tallawi, A. Grigore, A.R. Boccaccini, Synthesis, properties and biomedical applications of poly(glycerol sebacate) (PGS): a review, Prog. Polym. Sci. 37 (2012) 1051–1078, https://doi.org/10.1016/J.PROGPOLYMSCI.2012.02.001.

[25] X.J. Loh, A. Abdul Karim, C. Owh, Poly(glycerol sebacate) biomaterial: synthesis and biomedical applications, J. Mater. Chem. B 3 (2015) 7641–7652, https://doi.org/10.1039/C5TB01048A.

[26] L. Vogt, F. Ruther, S. Salehi, A.R. Boccaccini, Poly(Glycerol sebacate) in biomedical applications-A review of the recent Literature, Adv Healthc Mater 10 (2021), https://doi.org/10.1002/ADHM.202002026.

[27] K. Shukla, A study on the synthesis of various polyesters from glycerol, J. Polym. Res. 29 (2022), https://doi.org/10.1007/s10965-022-03221-0.

[28] M. Luginina, K. Schuhladen, R. Orrú, G. Cao, A.R. Boccaccini, L. Liverani, Electrospun PCL/PGS composite fibers incorporating bioactive Glass Particles for soft tissue engineering applications, Nanomaterials 10 (2020), https://doi.org/10.3390/NANO10050978, 978 10 (2020) 978.

[29] M. Rostamian, M.R. Kalaee, S.R. Dehkordi, M. Panahi-Sarmad, M. Tirgar, V. Goodarzi, Design and characterization of poly(glycerol-sebacate)-co-poly (caprolactone) (PGS-co-PCL) and its nanocomposites as novel biomaterials: the promising candidate for soft tissue engineering, Eur. Polym. J. 138 (2020) 109985, https://doi.org/10.1016/J.EURPOLYMJ.2020.109985.

[30] Z. Wu, K. Jin, L. Wang, Y. Fan, A review: optimization for poly(glycerol sebacate) and fabrication Techniques for its centered scaffolds, Macromol. Biosci. 21 (2021) 2100022, https://doi.org/10.1002/MABI.202100022.

[31] L. Yu, G. Zeng, J. Xu, M. Han, Z. Wang, T. Li, M. Long, L. Wang, W. Huang, Y. Wu, Development of poly(glycerol sebacate) and its Derivatives: a review of the progress over the past two Decades, Polym. Rev. 63 (2023) 613–678, https://doi.org/10.1080/15583724.2022.2150774.

[32] Q. Pan, Y. Guo, F. Kong, Poly(glycerol sebacate) combined with chondroitinase ABC promotes spinal cord repair in rats, J. Biomed. Mater. Res. B Appl. Biomater. 106 (2018) 1770–1777, https://doi.org/10.1002/JBM.B.33984.

[33] T. Olak, A. Turan, D. Alpaslan, T.E. Dudu, N. Aktaş, Developing poly(Agar-co-Glycerol-co-Thyme Oil) based organo-hydrogels for the controlled drug release applications, J. Drug Deliv. Sci. Technol. 60 (2020) 102088, https://doi.org/10.1016/J.JDDST.2020.102088.

[34] D. Alpaslan, T.E. Dudu, N. Aktaş, Synthesis and characterization of novel organo-hydrogel based agar, glycerol and peppermint oil as a natural drug carrier/release material, Mater. Sci. Eng. C 118 (2021) 111534, https://doi.org/10.1016/J.MSEC.2020.111534.

[35] X. Qi, C. Liu, J. Si, B. Yin, J. Huang, X. Wang, J. Huang, H. Sun, C. Zhu, W. Zhang, A bioenergetically-active ploy (glycerol sebacate)-based multiblock hydrogel improved diabetic wound healing through revitalizing mitochondrial metabolism, Cell Prolif. (2024), https://doi.org/10.1111/CPR.13613.

[36] K.J. Harber, K.E. de Goede, S.G.S. Verberk, E. Meinster, H.E. de Vries, M. van Weeghel, M.P.J. de Winther, J. Van den Bossche, Succinate is an Inflammation-induced Immunoregulatory metabolite in Macrophages, Metabolites 10 (2020) 372, https://doi.org/10.3390/METABO10090372, 372 10 (2020).

[37] H. Wang, B. Xia, M. Lin, Y. Wang, B. Sun, Y. Li, Succinic acid inhibits the activity of cytochrome P450 (CYP450) enzymes, Pharm. Biol. 58 (2020) 1150–1155, https://doi.org/10.1080/13880209.2020.1839110.

[38] D.D. Ojeda-Hernández, U. Gomez-Pinedo, M.A. Hernández-Sapiéns, A.A. Canales-Aguirre, H. Espinosa-Andrews, J. Matias-Guiu, Y. González-García, J.C. Mateos-Díaz, Biocompatibility of ferulic/succinic acid-grafted chitosan hydrogels for implantation after brain injury: a preliminary study, Mater. Sci. Eng. C 121 (2021) 111806, https://doi.org/10.1016/J.MSEC.2020.111806.

[39] K. Chen, C. Liu, J. Huang, L. Che, Y. Yuan, C. Liu, A Conformable and Tough Janus adhesive Patch with limited 1D swelling behavior for internal Bioadhesion, Adv. Funct. Mater. 33 (2023) 2303836, https://doi.org/10.1002/ADFM.202303836.

[40] E. Redondo-Castro, X. Navarro, G. García-Alías, Longitudinal evaluation of residual cortical and subcortical motor evoked potentials in spinal cord injured rats, J. Neurotrauma 33 (2016) 907–916, https://doi.org/10.1089/NEU.2015.4140/ASSET/IMAGES/LARGE/FIGURE6.JPEG.

[41] S.R. Mousavi, M.R. Farrokhi, M.K. Ghaffari, F. Karimi, S. Keshavarz, A. R. Dehghanian, M. Naseh, The combination treatment of methylprednisolone and growth factor-rich serum ameliorates the structural and functional changes after spinal cord injury in rat, Spinal Cord 62 (1 62) (2023) 17–25, https://doi.org/10.1038/s41393-023-00942-x, 2023.

[42] D. Krizsan-Agbas, M.K. Winter, L.S. Eggimann, J. Meriwether, N.E. Berman, P. G. Smith, K.E. McCarson, Gait analysis at multiple speeds reveals differential functional and structural outcomes in response to graded spinal cord injury, J. Neurotrauma 31 (2014) 846–856, https://doi.org/10.1089/NEU.2013.3115/ASSET/IMAGES/LARGE/FIGURE7.JPEG.

[43] D. Singh, A.J. Harding, E. Albadawi, F.M. Boissonade, J.W. Haycock, F. Claeyssens, Additive manufactured biodegradable poly(glycerol sebacate methacrylate) nerve guidance conduits, Acta Biomater. 78 (2018) 48–63, https://doi.org/10.1016/J.ACTBIO.2018.07.055.

[44] X. Lu, S. Shi, H. Li, E. Gerhard, Z. Lu, X. Tan, W. Li, K.M. Rahn, D. Xie, G. Xu, F. Zou, X. Bai, J. Guo, J. Yang, Magnesium oxide-crosslinked low-swelling citrate-based mussel-inspired tissue adhesives, Biomaterials 232 (2020) 119719, https://doi.org/10.1016/J.BIOMATERIALS.2019.119719.

[45] J. Li, H. Li, S. Cai, S. Bai, H. Cai, X. Zhang, CD157 in bone marrow mesenchymal stem cells mediates mitochondrial production and transfer to improve neuronal apoptosis and functional recovery after spinal cord injury, Stem Cell Res. Ther. 12 (2021) 1–14, https://doi.org/10.1186/S13287-021-02305-W/FIGURES/7.
[46] C.S. Mendes, I. Bartos, Z. Márka, T. Akay, S. Márka, R.S. Mann, Quantification of gait parameters in freely walking rodents, BMC Biol. 13 (2015) 1–11, https://doi.org/10.1186/S12915-015-0154-0/FIGURES/4.
[47] Z.Q. Jia, G. Li, Z.Y. Zhang, H.T. Li, J.Q. Wang, Z.K. Fan, G. Lv, Time representation of mitochondrial morphology and function after acute spinal cord injury, Neural Regen Res 11 (2016) 137–143, https://doi.org/10.4103/1673-5374.175061.
[48] K.Y. Morgan, D. Sklaviadis, Z.L. Tochka, K.M. Fischer, K. Hearon, T.D. Morgan, R. Langer, L.E. Freed, Multi-material tissue engineering scaffold with Hierarchical pore architecture, Adv. Funct. Mater. 26 (2016) 5873–5883, https://doi.org/10.1002/ADFM.201601146.
[49] A. Saudi, M. Rafienia, A. Zargar Kharazi, H. Salehi, A. Zarrabi, M. Karevan, Design and fabrication of poly (glycerol sebacate)-based fibers for neural tissue engineering: synthesis, electrospinning, and characterization, Polym. Adv. Technol. 30 (2019) 1427–1440, https://doi.org/10.1002/PAT.4575.
[50] D. Lin, B. Cai, L. Wang, L. Cai, Z. Wang, J. Xie, Q. xin Lv, Y. Yuan, C. Liu, S.G. Shen, A viscoelastic PEGylated poly(glycerol sebacate)-based bilayer scaffold for cartilage regeneration in full-thickness osteochondral defect, Biomaterials 253 (2020), https://doi.org/10.1016/J.BIOMATERIALS.2020.120095.
[51] D. Sha, Z. Wu, J. Zhang, Y. Ma, Z. Yang, Y. Yuan, Development of modified and multifunctional poly(glycerol sebacate) (PGS)-based biomaterials for biomedical applications, Eur. Polym. J. 161 (2021) 110830, https://doi.org/10.1016/J.EURPOLYMJ.2021.110830.
[52] M. Wang, S. Lin, M. Liu, J. Jiao, H. Mi, J. Sun, Y. Liu, R. Guo, S. Liu, H. Fu, Y. Yang, R. Li, An injectable and rapidly degraded carboxymethyl chitosan/polyethylene glycol hydrogel for postoperative antiadhesion, Chem. Eng. J. 463 (2023) 142283, https://doi.org/10.1016/J.CEJ.2023.142283.
[53] B.F. Zhao, F. Wang, J.C. Sun, J.P. Gao, L.J. Zhao, Z.L. Shen, Z.P. Li, Y.X. Wang, Y. Wang, D. Li, X.F. Mei, Revitalizing mitochondrial function and empowering spinal cord recovery using copper-catalyzed Pdots, Chem. Eng. J. 481 (2024) 148264, https://doi.org/10.1016/J.CEJ.2023.148264.
[54] B. Chen, Q. Tan, W. Zhao, Q. Yang, H. Zhang, F. Gao, X. Liu, H. Feng, D. Jiang, Diffusion tensor imaging and electrophysiology as robust assays to evaluate the severity of acute spinal cord injury in rats, BMC Neurol. 20 (2020) 1–10, https://doi.org/10.1186/S12883-020-01778-1/FIGURES/6.
[55] M.S. Lin, Y.H. Lee, W.T. Chiu, K.S. Hung, Curcumin provides neuroprotection after spinal cord injury, J. Surg. Res. 166 (2011) 280–289, https://doi.org/10.1016/J.JSS.2009.07.001.
[56] M. Tsintou, K. Dalamagkas, A.M. Seifalian, Advances in regenerative therapies for spinal cord injury: a biomaterials approach, Neural Regen Res 10 (2015) 726, https://doi.org/10.4103/1673-5374.156966.
[57] Z. Fan, X. Liao, Y. Tian, X. xuzhuzi, Y. Nie, A prevascularized nerve conduit based on a stem cell sheet effectively promotes the repair of transected spinal cord injury, Acta Biomater. 101 (2020) 304–313, https://doi.org/10.1016/J.ACTBIO.2019.10.042.
[58] Y. qing Wu, J. Xiong, Z. li He, Y. Yuan, B. ni Wang, J. yu Xu, M. Wu, S. su Zhang, S. fang Cai, J. xin Zhao, K. Xu, H. yu Zhang, J. Xiao, Metformin promotes microglial cells to facilitate myelin debris clearance and accelerate nerve repairment after spinal cord injury, Acta Pharmacol. Sin. 43 (6 43) (2021) 1360–1371, https://doi.org/10.1038/s41401-021-00759-5, 2021.
[59] H. Liu, D. Xiong, R. Pang, Q. Deng, N. Sun, J. Zheng, J. Liu, W. Xiang, Z. Chen, J. Lu, W. Wang, A. Zhang, Effects of repetitive magnetic stimulation on motor function and GAP43 and 5-HT expression in rats with spinal cord injury, J. Int. Med. Res. 48 (2020), https://doi.org/10.1177/0300060520970765/ASSET/IMAGES/LARGE/10.1177_0300060520970765-FIG5.JPEG.
[60] J. Luo, R. Borgens, R. Shi, Polyethylene glycol improves function and reduces oxidative stress in synaptosomal preparations following spinal cord injury, J. Neurotrauma 21 (2004) 994–1007, https://doi.org/10.1089/0897715041651097.
[61] J.K. Wang, Q. Guo, X.W. Zhang, L.C. Wang, Q. Liu, P.F. Tu, Y. Jiang, K.W. Zeng, Aglaia odorata Lour. extract inhibit ischemic neuronal injury potentially via suppressing p53/Puma-mediated mitochondrial apoptosis pathway, J. Ethnopharmacol. 248 (2020) 112336, https://doi.org/10.1016/J.JEP.2019.112336.
[62] H. Wei, L. Qu, S. Dai, Y. Li, H. Wang, Y. Feng, X. Chen, L. Jiang, M. Guo, J. Li, Z. Chen, L. Chen, Y. Zhang, Y. Chen, Structural insight into the molecular mechanism of p53-mediated mitochondrial apoptosis, Nat. Commun. 12 (1 12) (2021) 1–9, https://doi.org/10.1038/s41467-021-22655-6, 2021.
[63] A.G. Karadayian, A. Czerniczyniec, S. Lores-Arnaiz, Apoptosis due to after-effects of acute ethanol exposure in brain cortex: intrinsic and extrinsic signaling pathways, Neuroscience (2024), https://doi.org/10.1016/J.NEUROSCIENCE.2024.02.022.
[64] M. Li, The role of P53 up-regulated modulator of apoptosis (PUMA) in ovarian development, cardiovascular and neurodegenerative diseases, Apoptosis 26 (5 26) (2021) 235–247, https://doi.org/10.1007/S10495-021-01667-Z, 2021.
[65] H. Wei, H. Wang, G. Wang, L. Qu, L. Jiang, S. Dai, X. Chen, Y. Zhang, Z. Chen, Y. Li, M. Guo, Y. Chen, Structures of p53/BCL-2 complex suggest a mechanism for p53 to antagonize BCL-2 activity, Nat. Commun. 14 (1 14) (2023) 1–13, https://doi.org/10.1038/s41467-023-40087-2, 2023.